Biomed. Glasses 2019; 5:112–123 DE GRUYTER

Research Article

Louis Forto Chungong, Mark A. Isaacs, Alexander P. Morrell, Laura A. Swansbury, Alex C. Hannon, Adam F. Lee, Gavin Mountjoy, and Richard A. Martin*

Insight into the atomic scale structure of CaF_2-CaO-SiO_2 glasses using a combination of neutron diffraction, ^{29}Si solid state NMR, high energy X-ray diffraction, FTIR, and XPS

https://doi.org/10.1515/bglass-2019-0010
Received Aug 12, 2019; revised Oct 17, 2019; accepted Nov 03, 2019

Abstract: Bioactive glasses are important for biomedical and dental applications. The controlled release of key ions, which elicit favourable biological responses, is known to be the first key step in the bioactivity of these materials. Properties such as bioactivity and solubility can be tailored for specific applications. The addition of fluoride ions is particularly interesting for dental applications as it promotes the formation of fluoro-apatite. To date there have been mixed reports in the literature on how fluorine is structurally incorporated into bioactive glasses. To optimize the design and subsequent bioactivity of these glasses, it is important to understand the connections between the glass composition, structure and relevant macroscopic properties such as apatite formation and glass degradation in aqueous media. Using neutron diffraction, high energy X-ray diffraction, ^{29}Si NMR, FTIR and XPS we have investigated the atomic scale structure of mixed calcium oxide / calcium fluoride silicate based bioactive glasses. No evidence of direct Si-F bonding was observed, instead fluorine was found to bond directly to calcium resulting in mixed oxygen/fluoride polyhedra. It was therefore concluded that the addition of fluorine does not depolymerise the silicate network and that the widely used network connectivity models are valid in these oxyfluoride systems.

Keywords: Bioactive glass, fluoride, structure, network connectivity

***Corresponding Author: Richard A. Martin:** Aston Institute of Materials Research, School of Engineering & Applied Science, Aston University, Birmingham B4 7ET, United Kingdom; Email: R.A.Martin@Aston.ac.uk
Louis Forto Chungong, Alexander P. Morrell: Aston Institute of Materials Research, School of Engineering & Applied Science, Aston University, Birmingham B4 7ET, United Kingdom

1 Introduction

Bioactive glasses are important for biomedical and dental applications. These materials promote the formation of apatite, the mineral content of bone and enamel, through a process of ion dissolution followed by precipitation [1–3]. The addition of fluorine to bioactive glasses is potentially beneficial in preventing demineralisation, enhancing enamel remineralisation and preventing bacteria metabolism [4–6]. Fluoride ions in bioactive glasses are known to be beneficial for their antibacterial efficacy and promoting acidic resistance apatite [3, 7].

To understand, model and predict the behaviour of these glasses and ultimately improve their design, it is important to understand their structure. Ions are released from bioactive glasses under physiological conditions and the release of these biologically important ions are responsible for bioactivity. There is a strong correlation between the nature of the glass composition, its structure and network connectivity and the cross-linking density. Bioactive glasses are biodegradable providing a controlled release of Ca, P and Si ions [8]. High concentrations of calcium, released from the glass, combine with phosphorous either released by the glass and/or from body fluids and precipi-

Mark A. Isaacs: Aston Institute of Materials Research, School of Engineering & Applied Science, Aston University, Birmingham B4 7ET, United Kingdom; Department of Chemistry, University College London, London, WC1H 0AJ, United Kingdom; Harwell XPS, Research Complex at Harwell, Rutherford Appleton Laboratories, Didcot, OX11 0FA, United Kingdom
Laura A. Swansbury, Gavin Mountjoy: School of Physical Sciences, University of Kent, Canterbury, CT2 7NH, United Kingdom
Alex C. Hannon: ISIS facility, Science and Technology Facilities Council, Rutherford Appleton Laboratory, Harwell Science and Innovation Campus, Didcot, Oxfordshire, OX11 0QX, United Kingdom
Adam F. Lee: Applied Chemistry & Environmental Science, School of Science, RMIT University, Melbourne VIC 3000, Australia

Table 1: Nominal glass composition and densities, standard deviations in parenthesis

Glass code	Nominal glass composition (mol%)			Melting Temp. (°C)	Density (g/cm^3)
	SiO_2	CaO	CaF_2		
GF 3.3	48.4	48.4	3.3	1540	2.98(2)
GF 6.6	46.7	46.7	6.6	1530	2.97(4)
GF 9.3	45.3	45.3	9.3	1520	2.97(1)
GF 11.9	44.1	44.1	11.9	1510	2.99(3)
GF 16.1	41.9	41.9	16.1	1495	2.98(4)

tate to form apatite. Most studies to date have focused on 45S5 Bioglass®, and the structural role of calcium introduced in oxide form has been studied extensively and is well understood [9–12]. The addition of alkali or alkaline earth oxides depolymerises the glass network by breaking Si-O-Si bonds and thereby increasing dissolution, however the effect of introducing Ca in other forms such as CaF_2 is less well known.

Calcium has been successfully incorporated into glasses as CaF_2 to develop novel bioactive glasses for orthopaedic and dental implants, and for use in toothpaste [13]. In aqueous media fluoride doped bioactive glasses will form an acid resistant fluorapatite which is beneficial for dental applications [14, 15]. In designing novel bioactive glasses for biomedical applications, a fundamental understanding of how the glass composition affects its structure is key as this will impact on the resulting macroscopic properties. There are mixed reports on how fluorine is incorporated into the glass structure and even mixed reports on whether the incorporation of calcium fluoride is beneficial. Ebisawa *et al.* [16] reported suppressed apatite formation on CaO-SiO_2 glass surfaces through CaF_2 addition, finding that CaF_2 decreases the dissolution of calcium ions promoting the formation of a silica rich layer. Spectroscopic studies by Hayashi *et al.* [17] showed that CaF_2 in silicate glasses depolymerizes the silicate network forming Si-F bonds. Iwamoto *et al.* [18] also reported Si-F bonds are present for CaF_2 <7 mol%, however for CaF_2 >7 mol% they observed that fluorine bonds with Ca. Tsunawaka *et al.* [19] reported that CaF_2 depolymerises the silicate network for CaF_2 concentrations <15-20 mol% for CaO/SiO_2 <1, but ^{19}F NMR studies on CaO-CaF_2-SiO_2 glasses by Watanabe *et al.* [20] found that F was surrounded by ~4 calcium atoms with no detectable Si-F bonds for CaO/SiO_2 = 0.5 - 1.3 and 5 - 25 mol% CaF_2. Lusvardi *et al.* [21] reported ~2% Si-F bonds formed for CaF_2 content ≥ 20%. Here we report a detailed multi-technique structural investigation combining neutron diffraction, high energy X-ray diffraction, ^{29}Si solid-state NMR, FTIR and XPS with the objective of elucidating the structural role of fluorine in bioactive glasses.

2 Method

2.1 Glass preparation

Melt-quenched glass samples were prepared using SiO_2 (Alfa Aesar, 99.5%), CaF_2 (Alfa Aesar 99.5%) and $CaCO_3$ (Alfa Aesar, 99.96-100.05%) precursors. Each precursors was carefully weighed to give the appropriate molar concentrations and the chemicals were then thoroughly mixed before being placed into a 90% Pt - 10% Rh crucible. The crucible and precursors were then placed into a furnace at room temperature which was then heated at a rate of 10°C/minute under flowing argon to a final temperature between 1495°C and 1530°C. After homogenising for 1 h at this temperature, the liquids were rapidly splat-quenched between two graphite blocks to form glasses. To avoid potential absorption of moisture from air the glasses were stored in a desiccator. Glass densities were measured using helium pycnometry (Multipycnometer, Quantachrome Instruments). Nominal glass compositions are given in Table 1. As shown, glass compositions are written in the form $(CaO)_{50-x/2}(SiO_2)_{50-x/2}(CaF_2)_x$ where x varied between 3.3 and 16.1 mol%. This ensures a constant Si:O ratio to help highlight structural differences in the network caused by CaF_2 addition.

2.2 Neutron diffraction

Neutron diffraction spectra were collected using the GEneral Materials (GEM) diffractometer at the ISIS neutron and muon source, Rutherford Appleton Laboratory, UK [22]. The glass samples were coarsely ground and then loaded in a thin walled cylindrical 6 mm internal diameter vanadium container. Interference patterns were collected for each of the five bioactive glass samples as well as an empty vanadium container, a vanadium niobium null alloy (0.941 V: 0.059 Nb) and the empty GEM instrument which are necessary to perform the appropriate data corrections. All measurements were undertaken at ambient temperature. Data corrections including background scattering, inelastic, multiple and self-scattering were performed using GUDRUN [23]. Following these corrections, the resultant neutron diffraction interference function, $i(Q)$, is defined by

$$i(Q) = \sum_i \sum_j c_i c_j b_i b_j \left[p_{ij}(Q) - 1\right] \tag{1}$$

where c_i, c_j, b_i and b_j represent the atomic concentration and coherent scattering length of the chemical species i and j respectively, and $p_{ij}(Q)$ is the structure factor. Fourier transformation of $i(Q)$ generates the total correlation function, $T(r)$, given by

$$T(r) = T^0(r) + \frac{2}{\pi} \int_0^\infty Qi(Q) M(Q) \sin(Qr) dQ \tag{2}$$

where $M(Q)$ is a Lorch window function that considers the finite maximum experimentally attainable value of Q and $T^0(r)$ is the average density term, given by

$$T^o = 4\pi r \rho^o (\sum_i c_i b_i) \tag{3}$$

Important structural information can be obtained by modelling the real-space correlation functions. The pair functions are given by:

$$p_{ij}(Q)_{ij} = \frac{N_{ij} w_{ij}}{c_j} \frac{\sin Q r_{ij}}{Q r_{ij}} \exp\left[\frac{-Q^2 \sigma_{ij}^2}{2}\right] \tag{4}$$

where N_{ij}, r_{ij} and σ_{ij} represent the coordination number, atomic separation and disorder parameters respectively. The weighting factor w_{ij} is given by:

$$w_{ij} = 2 c_i c_j b_i b_j \quad \text{if } i \neq j \tag{5}$$

$$w_{ij} = c_i^2 b_i^2 \quad \text{if } i = j \tag{6}$$

Atomic bond distances, coordination numbers and the disorder parameters were fitted for the glasses using NXFit [24].

2.3 High energy X-ray diffraction

High energy X-ray diffraction data were collected at the I-15 beamline, Diamond Light Source, Harwell, UK. The instrument collected data in a 2θ geometry with a Si (311) Bent Laue monochromatic, E = 76.7 KeV, $\lambda = 0.162$ Å. This setup gave a 2θ range of 58° resulting in a Q_{max} of 38 Å^{-1}. Glass samples were ground into fine powders and loaded into silica glass capillaries with an inner diameter of 1.17 mm, an outer diameter of 1.5 mm, and a height of 40 mm. All measurements were conducted at room temperature and the measurement time per sample was 10 min. An empty capillary was measured for background corrections. The data was corrected for the empty capillary, normalisation, attenuation, absorption, Compton scattering, X-ray beam polarisation, Bremsstrahlung, fluorescence and subtraction of self-scattering term using the program GUDRUNX [25].

The total X-ray interference function $i^x(Q)$ is given as

$$i^x(Q) = \frac{I^{coh}(Q) - \left[\sum_{i=1}^n c_i f_i^2(Q)\right]}{\left[\sum_{i=1}^n c_i f_i(Q)\right]^2} \tag{7}$$

Fourier transforming the X-ray interference function yields the real space correlation $T^x(r)$ given as

$$T^x(r) = 4\pi r \rho^0 \left(\sum_i c_i \bar{a}_i\right)^2 + \frac{2}{\pi} \int_0^\infty Qi(Q) M(Q) \sin(Qr) dQ \tag{8}$$

where r is the distance from an arbitrary atom at the origin, ρ^0 is the number density in units of Å^{-3} and $\bar{a}_i$ is the atomic number. The resulting X-ray peak function for two distinct atomic species normalised with the sharpening function were produced with an X-ray weighting factor given as

$$w_{ij}^x = \frac{(2 - \delta_{ij}) c_i c_j f_i(Q) f_j(Q)}{\left|f_i(Q)\right|^2} \tag{9}$$

where δ_{ij} is the Kronekar delta function $\delta_{ij} = 1$ if $i = j$ and $\delta_{ij} = 0$ if $i \neq j$ while c_i, c_j, $f_i(Q)$, $f_j(Q)$ are the concentrations and form factors of two atomic species i, j respectively.

2.4 ^{29}Si NMR

Solid state NMR spectra were obtained at the EPSRC UK National Solid-state NMR service at Durham on a 4.0 mm pencil Varian VNMRS 400 MHz spectrometer. The observed ^{29}Si spectra were acquired with a frequency of 79.438 MHz, spectral width of 40322.6 Hz, acquisition time of 12.7 ms, and repetitions in the range 184-500 were accumulated with a recycling time of 120 s at ambient temperature. Direct excitation had a pulse duration of 5.0 µs with a two pulse phase modulated decoupling [26] spin rate of 8039 - 9128 Hz. Samples were referenced to neat tetramethysilane (0 ppm) [27].

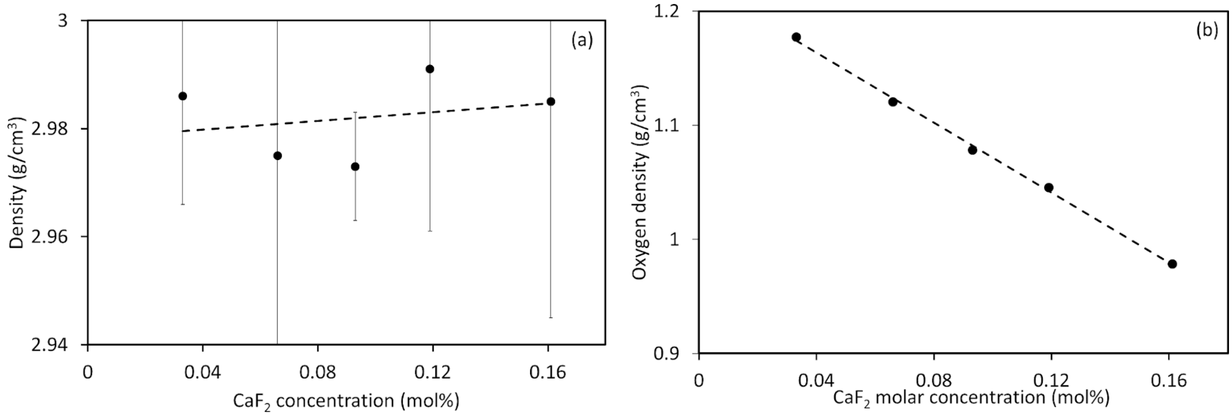

Figure 1: (a) Density and (b) oxygen density as a function of CaF_2 concentration

2.5 Fourier Transform Infrared spectroscopy

Fourier Transform Infrared (FTIR) spectroscopy was used to probe the local symmetry of the glass network, revealing structural information on the different vibrational modes present [28, 29]. Data was collected in transmission mode using a Thermo Nicolet IS50 infrared spectrometer with a single bounce diamond attenuated total reflection (ATR) crystal. Spectra were recorded in the range 400 - 4000 cm^{-1} with a step size of 0.05 cm^{-1}. All measurements were undertaken at room temperature. Each sample had 64 scans measured and the spectra was processed using OMNIC version 9.

2.6 X-ray photoelectron spectroscopy

Glass samples were affixed to the sample stage using carbon tape. Samples were evacuated until a pressure of 10^{-8} Torr was obtained. All data was recorded on a Kratos HSi spectrometer using a monochromated Al X-ray source (1486.7 eV). Sample alignment was performed using a z-scan at 1200 eV, with an X-ray power of 75 W and a step size of 0.05 mm. Survey spectra were recorded with a pass energy of 160 eV and X-ray power of 225 W. High resolution spectra were recorded with a pass energy of 20 eV and an X-ray power of 225 W. An electron flood gun was employed to neutralise charge accumulation. Data was analysed using CasaXPS v.2.3.19PR1.0. Data was energy calibrated to adventitious C 1s at 284.8 eV, Shirley background-subtracted and fitted with GL(30) lineshapes. Calcium 2p spectra were fitted using a 3.5 eV spin-orbit doublet separation and silicon 2p spectra using a 0.6 eV spin-orbit doublet separation. Quantitation was performed by integration of the high resolution spectra and application of instrument response factors.

3 Results

A series of calcium fluoride / calcium oxide silicate glasses were successfully prepared by splat quenching the melt between two graphite blocks. The glasses were visibly transparent with no obvious signs of crystallisation up to 16.1 mol% CaF_2. The amorphous nature of these materials was later confirmed by the absence of Bragg peaks in the X-ray and neutron diffraction data (presented below). Glasses with CaF_2 concentrations greater than 16.1 mol% predominantly crystallized upon quenching and were therefore discarded. It is challenging to measure the concentrations of oxygen and fluorine in glasses as these light elements are not easily detected. However, the weight of glass manufactured for each composition was as expected based on the weight of the starting batch and allowing for the loss of carbon dioxide from the calcium carbonate. This strongly suggested that there was no significant loss of CaF_2 or even SiF_4 (as previously reported). Hence we conclude that the nominal compositions in Table 1 are valid. Experimental glass densities for the present study are shown in Figure 1(a) and were approximately independent of CaF_2 content. These density results are in agreement with previous reports by Watanabe *et al.* [30] and Susa *et al.* [31] for similar composition glasses.

The corresponding oxygen density (Figure 1b) was obtained according to equation 10 [32, 33]

$$\rho^0 = \frac{M(O) \times (2Y_{SiO_2} + Y_{CaO})}{M_V} \tag{10}$$

where ρ^0 is the oxygen density, $M(O)$ is the molar mass of oxygen atom, Y is the molar concentration of the respective oxides and M_V is the molar volume of the glass. The oxygen density decreases linearly (R^2 = 0.9997) with CaF_2 content as expected.

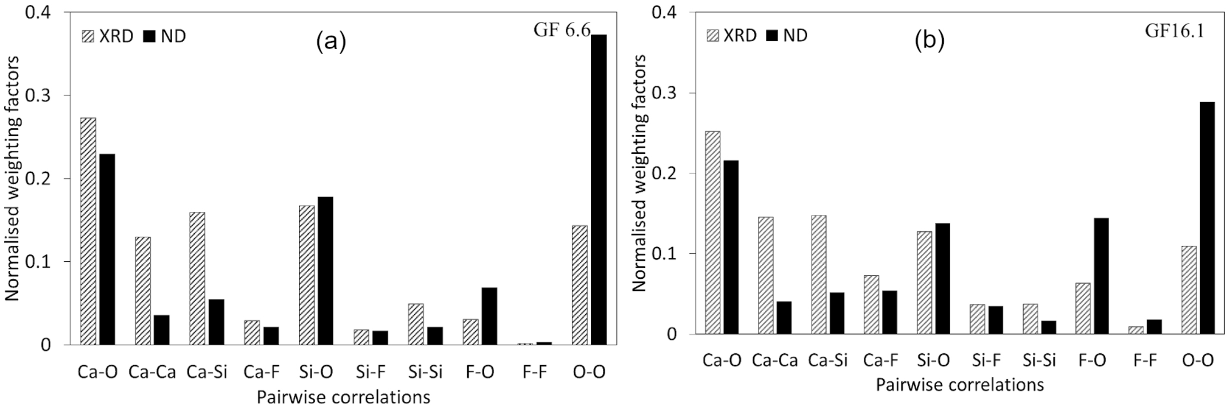

Figure 2: Relative weighting factors of neutrons and X-rays for the pairwise correlations in glasses GF 6.6 and GF 16.1

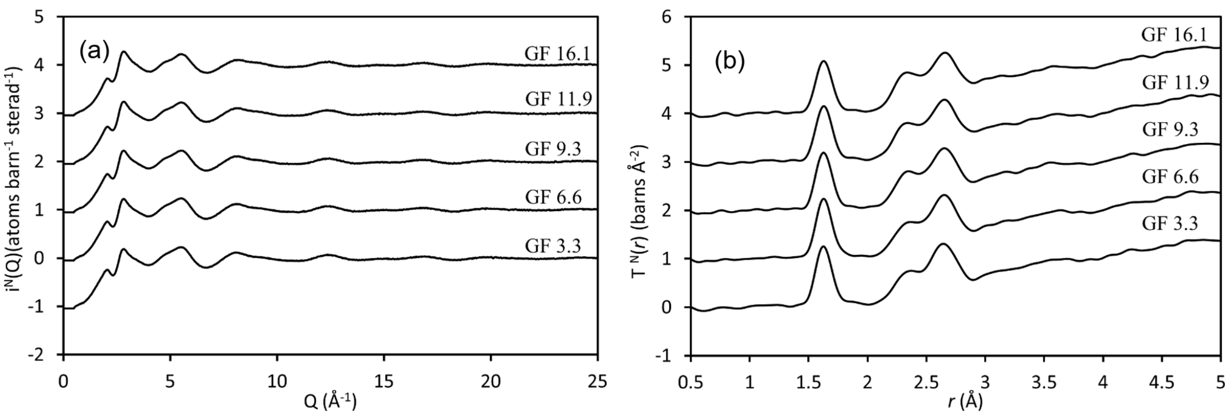

Figure 3: (a) Neutron diffraction reciprocal and (b) real space correlations for the fluoride glasses. Diffraction patterns offset for clarity

Normalised neutron and X-ray weighting factors for the glasses GF 6.6 and GF 16.1 are given in Figure 2. X-rays are more sensitive to heavy atoms, whilst neutron scattering is empirical with no direct correlation with atomic number. Neutron scattering was dominated by the O-O correlation, particularly for glasses with low CaF_2 concentrations, whereas X-ray scattering was more sensitive to calcium correlations.

Neutron diffraction interference functions i^N(Q) for the $(CaO)_{50-x/2}(SiO_2)_{50-x/2}(CaF_2)_x$ series are shown in Figure 3a. The reciprocal space data was modelled to Q_{max} = 50 Å^{-1} but is only shown out to 25 Å^{-1} for clarity. Figure 3b shows the corresponding real space data, T^N(r), obtained by Fourier transforming i^N(Q) over the full range (0<Q(Å^{-1})<50) using a Lorch modification function [35]. The X-ray interference functions i^X(Q) are shown in Figure 4a with the corresponding real space data, T^X(r), is shown in Figure 4b.

The shortest real space correlation ~1.6 Å is expected to correlate with Si-O bonds, however Si-F bonds (if present) would also occur in the same region overlapping with Si-O correlations. There is little variation in the coherent scattering lengths of O (b_c = 5.803 fm) and F (b_c = 5.654 fm) [36] which also makes it difficult to distinguish Si-O and Si-F correlations based solely on neutron diffraction data. The similarity in O and F atomic numbers also hinders differentiation of Si-O and Si-F by X-ray diffraction. Complimentary ^{29}Si solid state NMR spectroscopy is therefore required to resolve such correlations (Figure 5); spectra were similar for all glass compositions, exhibiting a broad peak at δ_{SiO} = −80.3 ppm (FWHM ~13 ppm) assigned as a Q^2 silicate [9, 34], of common intensity. These results do not preclude the presence of a small amount of Q^1/ Q^3 units, however significant Si-F bonds would induced a large distortion in the Si-O tetrahedra, resulting in a downfield NMR shift due to the high electronegativity of F^- relative to O^{2-}. We can therefore conclude that SiO_4 are in the same chemical environment in all samples, suggesting the absence of Si-F bonds.

IR bands around 850 cm^{-1} and 915 cm^{-1} are characteristic of Si-O silicate tetrahedra with two non-bridging and two bridging oxygens respectively [28, 29, 37]. FTIR spectra (Figure 6) of our glasses reveal bands at 850cm^{-1} and 898 cm^{-1}, which correlate well with those at 840-850

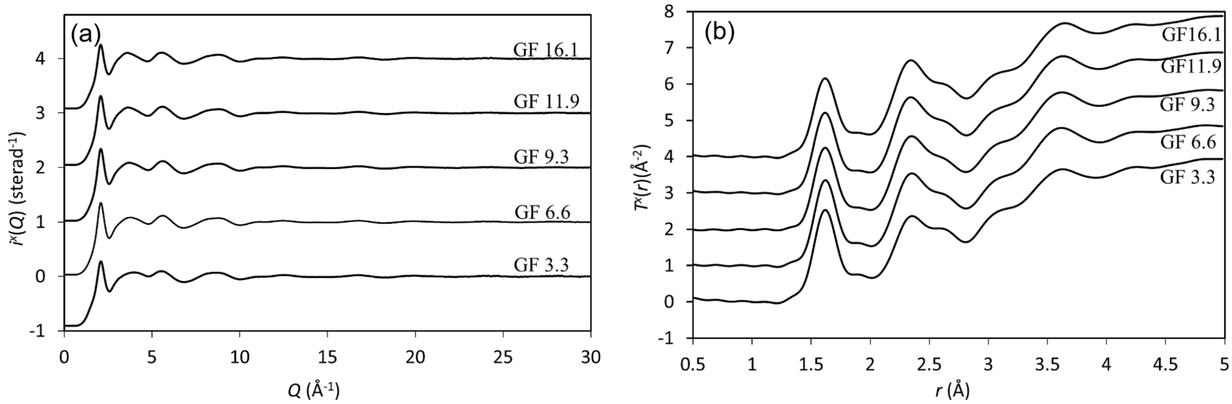

Figure 4: (a) X-ray diffraction reciprocal and (b) real space correlations for the fluoride glasses. Diffraction patterns offset for clarity

Table 2: F 1s and Ca 2p Binding energies (BE) and FWHM

Glass code	Ca $2p_{3/2}$ BE / eV (±0.2)	Ca $2p_{1/2}$	FWHM / eV	Si 2p BE / eV	FWHM / eV	F 1s BE / eV (±0.2)	FWHM / eV
GF 3.3	348.4	351.4	3.5	102.5	2.05	685.4	2.8
GF 6.6	348.3	351.4	3.1	102.2	2.02	685.3	2.7
GF 9.3	348.1	351.4	3.3	102.4	2.1	685.1	2.6
GF 11.9	347.5	351.6	3.2	102.4	1.9	685.0	2.7
GF 16.1	347.5	351.4	3.4	102.2	2.05	685.2	3.1

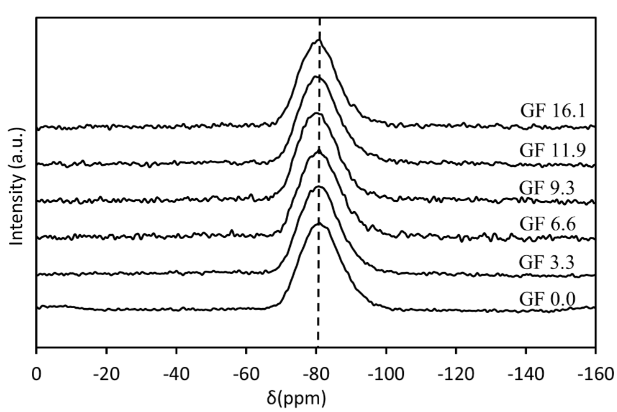

Figure 5: Solid state ^{29}Si MAS NMR data

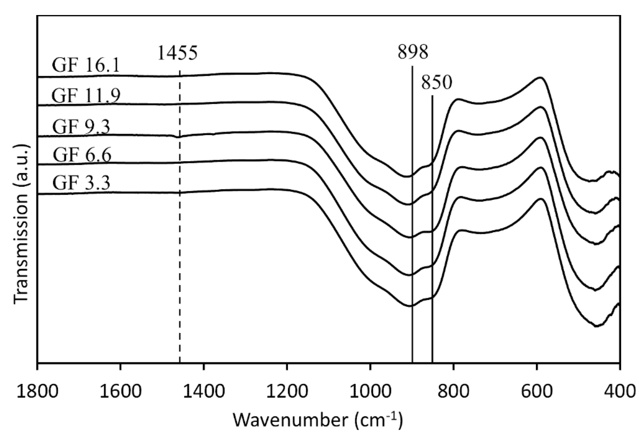

Figure 6: FTIR spectra for the glass series. Si-F features would be expected ~940 cm^{-1}

cm^{-1} and 920 cm^{-1} [28, 38, 39] previously reported for Q^2 metasilicate chains. Q^3 vibrations are typically observed between 890-975 cm^{-1} [37] while Si-F bonds are expected at 940 cm^{-1} [40, 41]; the absence of any such well-resolved feature in our spectra support NMR observations that there is a minimal direct Si-F bonding. Note that Q^2 and Q^3 features may also overlap in IR spectra complicating spectral interpretation. The very weak band ~1455 cm^{-1} in GF 9.3 is attributed to C-O stretches [28] possibly resulting from quenching of the glass on a graphite block.

Figure 7 shows the Ca 2p, Si 2p and F 1s XP spectra, with corresponding binding energies and FWHM shown in Table 2. The chemical environment of all elements was approximately independent of CaF_2 content. Calcium exhibited two peaks associated with the $2p_{3/2}$ and $2p_{1/2}$ spin-orbit split doublet at 347.5 eV and 351 eV binding energies respectively (Figure 7a); the former broad $2p_{3/2}$ photoemission was significantly higher than typical for calcium oxide (346.6 eV) [42], and lower than observed for calcium fluoride (348.4) [43]. For calcium silicate the emission re-

Table 3: Neutron diffraction structural parameters obtained by fitting T^N(r)

Glass	SiO			CaO_{NB}			O-(Si)-O			CaO_B			CaF		
	r(Å)	N	σ(Å)	r(Å)	N	σ(Å)	r(Å)	N	σ(Å)	r(Å)	N	σ(Å)	r(Å)	N	σ(Å)
GF 3.3	1.63	3.9	0.06	2.37	5.3	0.14	2.66	4.0	0.09	2.76	1.4	0.05	2.27	0.3	0.12
GF 6.6	1.63	3.9	0.06	2.37	5.1	0.14	2.66	4.1	0.10	2.73	1.4	0.10	2.25	0.5	0.11
GF 9.3	1.63	3.9	0.06	2.37	4.7	0.13	2.66	4.1	0.10	2.73	1.4	0.10	2.23	0.7	0.15
GF11.9	1.63	4.0	0.06	2.37	4.7	0.13	2.66	4.1	0.10	2.74	1.3	0.10	2.24	0.9	0.17
GF16.1	1.63	4.1	0.06	2.37	4.5	0.13	2.67	4.1	0.10	2.71	1.2	0.10	2.26	1.2	0.18

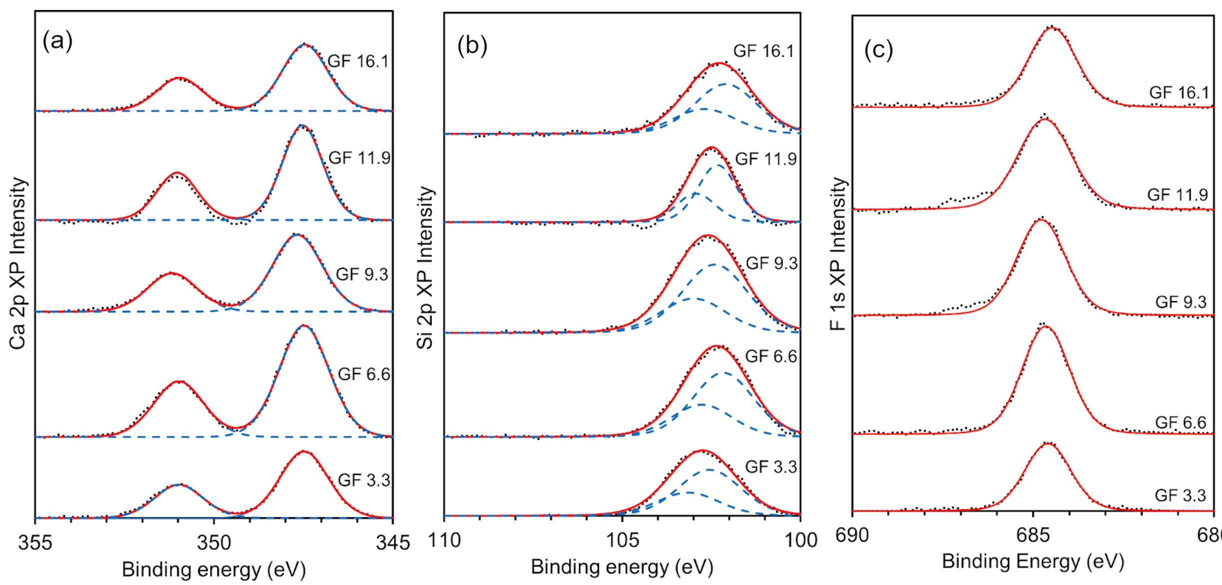

Figure 7: (a) Ca 2p and (b) Si 2p and (c) F 1s XP spectra. Dotted lines indicate raw spectra, dashed lines indicate the fitted peak envelopes, and the solid red line represents the overall fit

ported with a binding energy of ~347.2 eV [43], and so we postulate that the majority of Ca in our materials is present as the silicate or in a mixed oxide/fluoride environment. The F 1s binding energy of ~684.5 eV (Figure 7c) is similar to that in crystalline CaF_2 (684.3 eV) [44]; previous studies suggest that F in covalent Si-F bonds has a binding energy of 687.1 eV [45], of which there is no evidence in our glasses. We conclude that F bonds predominantly to Ca and does not change the nature of silicate network at CaF_2.

Returning to the diffraction patterns (Figures 3 and 4), real space correlations can now be modelled. In the absence of direct Si-F bonds, the first (shortest distance) diffraction peak was modelled assuming only Si-O correlations. Figure 8 shows neutron diffraction fits for the GF 6.6 and GF 16.1 glass samples and individual atomic partial pair correlations as representative fits; structural parameters from fitting T^N(r) are given in Table 3. The Si-O peak is well resolved with peak positions ~1.63 Å and coordination numbers ~4.0(1) for all the glass compositions, confirming that Si-O tetrahedra are unaffected by CaF_2 addition. The Si-O peak positions and coordination numbers are similar to previous reports for fluoride-free bioactive glasses [9, 34].

The second larger real space feature (2<r(Å)<3) corresponds to O-(Si)-O and Ca-O correlations. As previously reported, the Ca-O correlation comprises a shorter non-bridging (Ca-O_{NB}) and longer bridging (Ca-O_B) contribution [9]. Ca-F correlations are also anticipated in this region [30], the Ca-O structure, bond distances and coordination number is extremely diverse in related crystalline structures [46]. For example in cuspidine ($Ca_4F_2Si_2O_7$) Ca has three distinct sites with coordination numbers of 7, 7, 8 [47] and in crystalline β-$CaSiO_3$ the coordination numbers are 6, 6 and 7 respectively [12]. For a silicate tetrahedron, using simply geometry, the O-(Si)-O distance is expected to occur at $\sqrt{\frac{8}{3}}r_{si-o} \approx 2.65$ Å [34]. Using the network connectivity model (which we now know to be valid since the addition of fluorine does not disrupt the network connectivity) the O-(Si)-O coordination number can be calculated using the Q^n value determined from ^{29}Si NMR. For

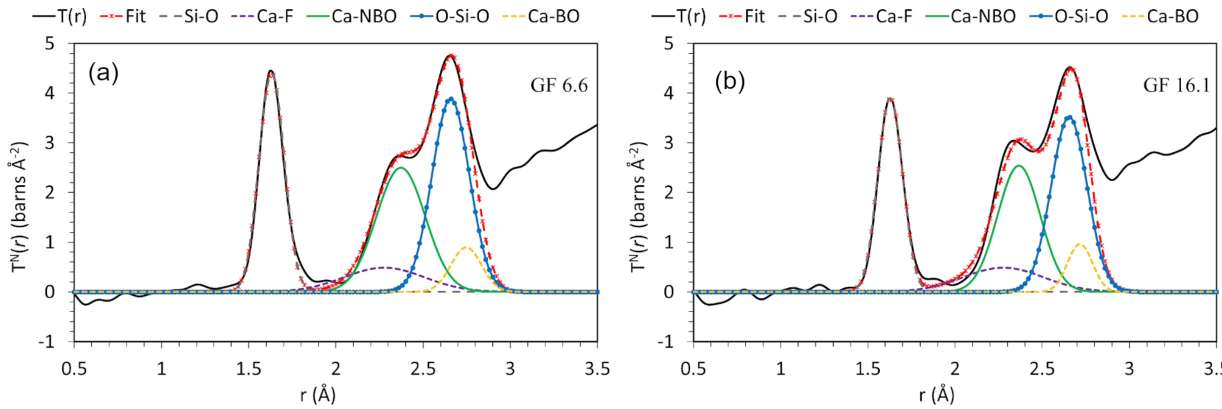

Figure 8: The real-space total diffraction patterns, $T^N(r)$, and the individually fitted pair correlation functions for GF 6.6 and GF 16.1. Colour online

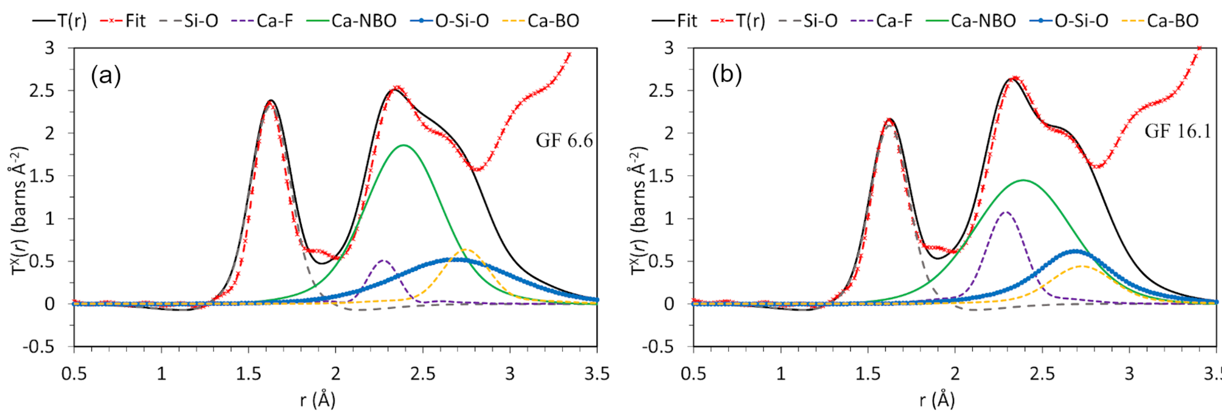

Figure 9: The real-space total diffraction patterns, $T^X(r)$, and the individually fitted pair correlation functions for GF 6.6 and GF 16.1. Colour online

Table 4: High energy X-ray diffraction output parameters obtained from fitting $T^X(r)$

Glass	SiO			CaO_{NB}			O-(Si)-O			CaO_B			CaF		
	r(Å)	N	σ(Å)	r(Å)	N	σ(Å)	r(Å)	N	σ(Å)	r(Å)	N	σ(Å)	r(Å)	N	σ(Å)
GF 3.3	1.63	3.8	0.09	2.39	5.1	0.25	2.66	4.0	0.26	2.77	1.2	0.15	2.29	0.3	0.03
GF 6.6	1.63	3.8	0.09	2.39	4.9	0.20	2.68	4.0	0.28	2.72	1.2	0.12	2.27	0.4	0.05
GF 9.3	1.63	3.8	0.09	2.37	4.6	0.18	2.68	3.9	0.26	2.75	1.3	0.12	2.24	0.5	0.11
GF11.9	1.63	3.8	0.09	2.39	4.6	0.26	2.68	3.9	0.24	2.75	1.2	0.10	2.26	0.7	0.11
GF16.1	1.63	3.9	0.08	2.39	4.5	0.26	2.68	3.9	0.17	2.73	1.1	0.17	2.29	1.1	0.09

Q^2 species, a non-bridging oxygen has three nearest neighbours and a bridging oxygen has six nearest neighbours. It can therefore be calculated that the O-(Si)-O coordination in a Q^2 species has a coordination number of four at 2.65Å. The complex overlapping correlation around $2 < r$ (Å) < 2.8 has therefore been simplified using Q^n speciation in conjunction with a network connectivity model, and verified by ^{29}Si NMR.

To enable direct comparison between the X-ray diffraction and neutron diffraction data, the X-ray real space functions were fitted by using the output parameters from neutron diffraction as nominal input parameters. During fitting the input parameters were allowed to vary until an optimsed best fit was obtained. The resultant X-ray fits are given in Figure 9, and the corresponding output structural parameters in Table 4. As seen in Table 4, the first peak corresponds to a Si-O correlation with R_{Si-O} = 1.63 Å and coordination number between 3.8-3.9 in all the glasses. Ca-F distances of 2.24 - 2.29 Å agree with those from neutron diffraction (Table 3). Ca-O_{NB} distances are ~2.37-2.39 Å, and the Ca-O_{NB} coordination number decreases from 5.1 to 4.6(2) with CaF_2 content. Ca-O_B distances are ~2.73-2.77 Å with an O_B average coordination decreasing from 1.3 to 1.1 with CaF_2 content. The X-ray partial pair structure factors in Figure 9 are broader than those for neutron diffraction because of a lower real space resolution imposed on Q_{max} = 30 Å^{-1} compared to neutron diffraction Q_{max} = 50Å^{-1}, nevertheless there is good agreement between the X-ray and neutron data sets.

4 Discussion

Most bioactive glasses are oxide based, and consequently their bioactivity and dissolution are typically characterised using network connectivity calculations based on the concentration of network formers (*i.e.* silicon) and oxygen atoms. For example, the network connectivity (NC) of an oxide based silicate glass can be described as

$$NC = 4 - 2Z, \qquad (11)$$

where Z, the number of excess oxygen atoms per SiO_2, is given by

$$Z = \frac{c_O}{c_{Si}} - 2 \qquad (12)$$

where c_O and c_{Si} represent the concentration of oxygen and silicon respectively [9, 34]. However, it is unclear whether these equations remain valid for bioactive glasses containing halides. If fluoride (or chloride) ions directly bind to silicon this will result in network depolymerisation, reducing the network connectivity and increasing the rate of dissolution and consequent (possible) bioactivity.

No evidence was found that CaF_2 addition to silica glasses results in Si-F bonds. Solid state ^{29}Si MAS NMR data do not evidence a chemical shift, indicating that F is not directly bonded to Si. FTIR also shows no evidence of Si-F bonds. Diffraction experiments reveal Ca-F correlations at 2.23-2.27 Å for x = 3.3 - 16.1 (Tables 3 and 4) with Ca-F coordination numbers varying from 0.3 to 1.2 with increasing CaF_2. Ca-O_{NB} and Ca-O_B correlations were observed at 2.37 Å and ~2.71-2.76 Å, consistent with previous reports for halide-free bioactive glasses, and recent publications for calcium chloride containing bioactive glasses. Calcium was surrounded by between 5.3 to 4.5(2) O_{NB}, while the number of O_B decreased from 1.4 to 1.2(1) upon CaF_2 addition (Figure 10). The Ca-O values for the dilute CaF_2 glass (GF 3.3) agree with previous reports for fluoride-free bioactive calcium silicate glasses [48, 49]. For the remaining glasses, a reduction in Ca-O coordination number occurs due to the replacement of O by F. The Ca-O bond

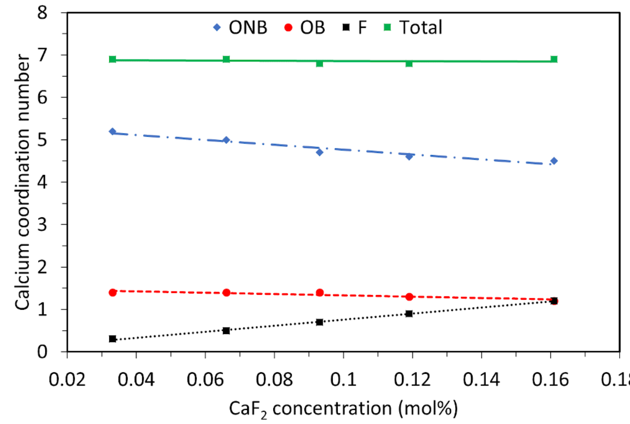

Figure 10: Calcium coordination number as a function of CaF_2 content

distances obtained herein are in good agreement with Ca-O_{NB} and Ca-O_B bond distances at 2.37 Å and 2.78 Å respectively in $CaCl_2$-CaO-SiO_2 glasses [50, 51], and in halide-free bioactive glasses where Ca-O_{NB} and Ca-O_B distances range from 2.32 to 2.76 Å [9, 34, 48]. Direct comparison of the Ca-O bond distances showed agreement with those in crystalline calcium fluorosilicate ($Ca_4Si_2O_7F_2$) wherein Ca-O distances lie between 2.28 and 2.76 Å with Ca in a mixed coordination environment of four oxygen and three fluorine atoms [47].

As expected, the average Ca-F coordination number increases with CaF_2 content while the total Ca-O coordination number decreases. The total O and F atoms around calcium remains constant at ~7, in agreement with that of Ca polyhedra in crystalline cuspidine ($Ca_2F_2Si_2O_7$). To allow direct comparison with fluoride-free bioglasses, the CaO/CaF coordination numbers were scaled according to the molar concentrations of F and O; this scaling allows direct comparison with halide-free bioactive glasses systems [9, 34, 50]. The scaled Ca-O_{NB} and Ca-O_B coordination numbers are close to those of GF 3.3 (lowest CaF_2 concentration). Conventional halide free network connectivity models (given in equations 11 and 12) predict a Q^2 structure for the present fluoride glasses, and therefore assume that fluorine does not interact with the silica network. The $(CaO)_{50-x/2}(SiO_2)_{50-x/2}(CaF_2)_x$ series have a Si:O molar ratio of 1:3 ratio (Table 1), consistent with one excess oxygen per SiO_2 unit (*i.e.* Z=1). It is therefore anticipated that these glasses adopt a Q^2 structure, if fluorine does not directly bond with silicon.

Bond valence theory can be used to verify reliabilities of the Ca-F and Ca-O bond distances and calcium coordination numbers [52]. The oxidation state of a cation can be

Table 5: Average individual calcium coordination numbers determined by neutron diffraction and bond valence of calcium

Glass code	Coordination numbers				Valence Sum
	Ca-O_{NB}	Ca-O_B	Ca-F	Ca-(O_{NB}+F)	
GF 3.3	5.2	1.3	0.3	5.5	2.00
GF 6.6	5.0	1.3	0.5	5.5	2.02
GF 9.3	4.7	1.3	0.7	5.4	2.00
GF 11.9	4.6	1.3	0.9	5.5	1.98
GF 16.1	4.5	1.2	1.2	5.7	2.00

calculated using equation (13).

$$V_i = \sum_j v_{ij} = \sum_j exp\left[\frac{R_{ij}-r_{ij}}{B}\right] \quad (13)$$

where v_{ij} is the bond valence between atom i and j, B is an empirical constant (0.37) and R_{ij} is the bond valence parameter for the atom pair i, j. R_{ij} values of R_{CaO} = 1.967 Å and R_{CaF} = 1.842 Å are reported by Bresse and O'Keefee [53]. R_{ij}values for r_{Ca-NBO}, r_{Ca-BO} and r_{Ca-F} determined from neutron diffraction data are given in Table 4, and calculated valences in Table 5. Values of ~2.00(2) were calculated for all bioactive glass compositions, consistent with Ca^{2+} cations, and further verifying the reliability of Ca-O and Ca-F bond distances and coordination numbers obtained from neutron and X-ray co-fitting.

5 Conclusions

A combination of neutron, high energy X-ray diffraction, NMR, XPS, FTIR and XRD have been used to study the structure of fluoride bioactive silicate glasses. The Si-O coordination number remained ~4.0 for all samples, with no change in the disordering. No distortions in the total correlation functions of $T^N(r)$, $T^X(r)$ were observed for SiO_4 tetrahedra following CaF_2 addition, discounting possible direct Si-F bonding. It is therefore concluded that F does not depolymerise the silicate network or change the glass network connectivity, even at very low CaF_2 content. The absence of Si-F bonding was confirmed by the XPS spectra and ^{29}Si NMR spectroscopy, with a $\delta_{SiO} = -80.3$ ppm evidencing undistorted SiO_4 tetrahedra, showing that Si-O-Si connectivity was independent of CaF_2 addition into the glass; CaF_2 does not impact the silicate network. Increasing the CaF_2 concentration decreases the average Ca-O_B coordination, with a weaker decreases in Ca-O_{NB}, however the total Ca-O/F polyhedra remained constant ~6.8(1). Widely used network connectivity models, developed for oxide based glasses, appear valid for these mixed oxide / fluoride glass systems.

Acknowledgement: The authors thank STFC for the provision of beam-time at the ISIS pulsed neutron source [1620417], the Diamond Light Source for provision of X-ray beam-time at I15-1 [reference EE16079-1] and the Solid State NMR service, University of Durham, for solid state NMR experiments. The authors would like to thank Dean Kebble for assistance with the I-15 High Energy X-ray Diffraction experiments at the Diamond Light Source. The authors also thank R.G. Hill and N. Karpukhina for helpful scientific discussions. This publication is derived from Dr Louis Forto Chungong's PhD thesis.

Conflict of Interests: There is no conflict of interest regarding the publication of this paper

Ethical approval: The conducted research is not related to either human or animals use

References

[1] El Batal F.H., El-Bassyouni G.T., Bioactivity of Hench bioglass and corresponding glass-ceramic and the effect of transition metal oxides, Silicon, 2011, 3(4), 185-197.
[2] Hench L.L., Bioceramics, a clinical success, Amer. Ceram. Soc. Bull., 1998, 77(7), 67-74.
[3] Shah F.A., Fluoride-containing bioactive glasses: Glass design, structure, bioactivity, cellular interactions, and recent developments, Mater. Sci. Eng. C, 2016, 58, 1279-1289.
[4] Thuy T.T. et al., Effect of strontium in combination with fluoride on enamel remineralisation in vitro, Archiv. Oral Biol., 2008, 53(11), 1017-1022.
[5] Brauer D. et al., Fluoride-containing bioactive glass-ceramics. J. Non-Crystall. Solids, 2012, 358(12-13), 1438-1442.
[6] Featherstone J.D., The Sci. and practice of caries prevention, J. Amer. Dent. Assoc., 2000, 131(7), 887-899.
[7] Caverzasio J., Palmer G., Bonjour J.-P., Fluoride: mode of action. Bone, 1998, 22(6), 585-589.
[8] Jones J.R. et al., Controlling ion release from bioactive glass foam scaffolds with antibacterial properties, J. Mater. Sci.: Mater. Med., 2006, 17(11), 989-996.
[9] Martin R. et al., An examination of the calcium and strontium site distribution in bioactive glasses through isomorphic neutron

diffraction, X-ray diffraction, EXAFS and multinuclear solid state NMR, J. Mater. Chem., 2012, 22(41), 22212-22223.

[10] Mead R., G. Mountjoy, The structure of CaSiO3 glass and the modified random network model, Phys. Chem. Glasses, 2005, 46(4), 311-314.

[11] Newport R.J. et al., In vitro changes in the structure of a bioactive calcia–silica sol–gel glass explored using isotopic substitution in neutron diffraction, J. Non-crystall. Solids, 2007, 353(18), 1854-1859.

[12] Lin Z. et al., Probing the local structural environment of calcium by natural-abundance solid-state Ca 43 NMR, Phys. Rev. B, 2004, 69(22), 224107.

[13] Davari A., E. Ataei, and H. Assarzadeh, Dentin hypersensitivity: etiology, diagnosis and treatment; a literature review, J. Dentistry, 2013, 14(3), 136.

[14] Jha L. et al., Preparation and characterization of fluoride-substituted apatites, J. Mater. Sci.: Mater. in Med., 1997, 8(4), 185-191.

[15] Brauer D.S. et al., Density-structure correlations in fluoride-containing bioactive glasses. Mater. Chem. Phys., 2011. 130(1), 121-125.

[16] Ebisawa Y. et al., Bioactivity of $CaO \cdot SiO_2$-based glasses: in vitro evaluation, J. Mater. Sci.: Mater. Med., 1990, 1(4), 239-244.

[17] Hayashi M. et al., Effect of fluorine on silicate network for CaO-CaF_2-SiO_2 and CaO-CaF_2-SiO_2-FeOx glasses, ISIJ Int., 2002, 42(4), 352-358.

[18] Iwamoto N., Makino Y., A structural investigation of calcium fluorosilicate glasses, J. Non-Crystall. Solids, 1981, 46(1), 81-94.

[19] Tsunawaki Y. et al., Analysis of CaO-SiO_2 and CaO-SiO_2-CaF_2 glasses by Raman spectroscopy, J. Non-Crystalline Solids, 1981, 44(2-3), 369-378.

[20] Watanabe T. et al., Solid-state 19F NMR on CaO-SiO_2-CaF_2 glasses, Johannesburg: The South Afr. Inst. Mining Metall., 2004, 699-706.

[21] Lusvardi G. et al., Elucidation of the structural role of fluorine in potentially bioactive glasses by experimental and computational investigation, J. Phys. Chem. B, 2008, 112(40), 12730-12739.

[22] Hannon A.C., Results on disordered Mater. from the GEneral Mater. diffractometer, GEM, at ISIS, Nuclear Instruments & Methods in Physics Research Section a-Accelerators Spectrometers Detectors and Associated Equipment, 2005, 551(1), 88-107.

[23] McLain S. et al., GUDRUN, a computer program developed for analysis of neutron diffraction data. ISIS Facility, Rutherford Appleton Laboratory, Chilton, UK.

[24] Pickup D., R. Moss, and R. Newport, NXFit: a program for simultaneously fitting X-ray and neutron diffraction pair-distribution functions to provide optimized structural parameters, J. Appl. Crystall., 2014, 47(5), 1790-1796.

[25] Soper A.K., GudrunN and GudrunX: programs for correcting raw neutron and X-ray diffraction data to differential scattering cross section, 2011, Sci. & Technol. Facilities Council.

[26] Bennett A.E. et al., Heteronuclear decoupling in rotating solids, J. Chem. Phys., 1995, 103(16), 6951-6958.

[27] Harris R.K. et al., NMR nomenclature: nuclear spin properties and conventions for chemical shifts. IUPAC Recommendations 2001. International Union of Pure and Applied Chemistry. Physical Chemistry Division. Commission on Molecular Structure and Spectroscopy, Magn. Res. Chem., 2002, 40(7), 489-505.

[28] Aguiar H. et al., Structural study of sol–gel silicate glasses by IR and Raman spectroscopies, J. Non-Crystall. Solids, 2009, 355(8), 475-480.

[29] Serra J. et al., Influence of the non-bridging oxygen groups on the bioactivity of silicate glasses, J. Mater. Sci.: Mater. in Med., 2002, 13(12), 1221-1225.

[30] Watanabe T. et al., Solid-state 19F NMR on CaO-SiO_2-CaF_2 glasses, Johannesburg: The South Afr. Inst. Mining Metall., 2004, 699-706.

[31] Susa M., Sakamaki T., Kojima R., Chemical states of fluorine in CaF_2-CaO–SiO_2 and NaF-Na_2O-SiO_2 glassy slags from the perspective of electronic polarisability, Ironmaking & Steelmaking, 2005, 32(1), 13-20.

[32] Fredholm Y.C. et al., Strontium containing bioactive glasses: glass structure and physical properties, J. Non-Crystall. Solids, 2010, 356(44), 2546-2551.

[33] Fernandes H.R. et al., Structure, properties and crystallization of non-stoichiometric lithium disilicate glasses containing CaF_2, J. Non-Crystall. Solids, 2014. 406, 54-61.

[34] Martin R.A. et al., A structural investigation of the alkali metal site distribution within bioactive glass using neutron diffraction and multinuclear solid state NMR, Phys. Chem. Chem. Phys., 2012, 14(35), 12105-12113.

[35] Lorch E., Neutron diffraction by germania, silica and radiation-damaged silica glasses, J. Phys. C: Solid State Phys., 1969, 2(2), 229.

[36] Sears V.F., Neutron scattering lengths and cross sections, Neutron News, 1992, 3(3), 26 - 37.

[37] Serra, J. et al., FTIR and XPS studies of bioactive silica based glasses. J. Non-Crystall. Solids, 2003, 332(1), 20-27.

[38] Lynch E. et al., Multi-component bioactive glasses of varying fluoride content for treating dentin hypersensitivity, Dent. Mater., 2012, 28(2), 168-178.

[39] Chen X. et al., Bioactivity of sodium free fluoride containing glasses and glass-ceramics. Materials, 2014, 7(8), 5470-5487.

[40] Yoshimaru M., Koizumi S., Shimokawa K., Structure of fluorine-doped silicon oxide films deposited by plasma-enhanced chemical vapor deposition, J. Vacuum Sci. & Technol. A: Vacuum, Surfaces, and Films, 1997, 15(6), 2908-2914.

[41] Ding S.-J. et al., Structure characterization of carbon and fluorine-doped silicon oxide films with low dielectric constant, Mater. Chem. Phys., 2001, 71(2), 125-130.

[42] Demri B. and D. Muster, XPS study of some calcium compounds, J. Mater. Process. Technol., 1995, 55(3), 311-314.

[43] Black L. et al., X-ray photoelectron spectroscopic investigation of nanocrystalline calcium silicate hydrates synthesised by reactive milling, Cement Concr. Res., 2006, 36(6), 1023-1031.

[44] Hayakawa S. et al., An x-ray photoelectron spectroscopic study of the chemical states of fluorine atoms in calcium silicate glasses. J. Mater. research, 1998. 13(03), 739-743.

[45] Fujii E. et al., Structure and biomineralization of calcium silicate glasses containing fluoride ions, J. Ceram. Soc. Jap.2003, 111(1298), 762-766.

[46] Martin R.A. et al., Characterizing the hierarchical structures of bioactive sol–gel silicate glass and hybrid scaffolds for bone regeneration, Phil. Trans. R. Soc. A, 2012, 370(1963), 1422-1443.

[47] Saburi S. et al., The refinement of the crystal structure of cuspidine, Mineralog. J., 1977, 8(5), 286-298.

[48] Smith J.M. et al., Structural characterisation of hypoxia-mimicking bioactive glasses. J. Mater. Chemistry B, 2013, 1(9), 1296-1303.

[49] Martin R.A. et al., Structural characterization of titanium-doped Bioglass using isotopic substitution neutron diffraction, Phys. Chem. Chem. Phys., 2012, 14(45), 15807-15815.
[50] Chungong L.F. et al., Atomic structure of chlorine containing calcium silicate glasses by neutron diffraction and 29Si solid state NMR, Int. J. Appl. Glass Sci., 2017,
[51] Swansbury L.A. et al., Modeling the Onset of Phase Separation in CaO-SiO_2-$CaCl_2$ Chlorine-Containing Silicate Glasses, J. Phys. Chem. B, 2017, 121(22), 5647-5653.
[52] Brown I.D., Altermatt D., Bond-valence parameters obtained from a systematic analysis of the inorganic crystal-structure database, Acta Crystall. Sect. B-Structural Sci., 1985. 41(AUG), 244-247.
[53] Brese N., O'keeffe M., Bond-valence parameters for solids, Acta Crystall. Sect. B: Structural Sci., 1991, 47(2), 192-197.